Chapter 3

Transition Edge Sensor Bolometers

3.1 Introduction

Transition Edge Sensor (TES) bolometers have enabled large detector arrays for several applications, including CMB measurements. Experiments such as SPT and ACT succeeded in their goals largely because of this technology and up-coming CMB polarimetry will depend on it as well. All millimeter devices fabricated and tested in this thesis used TES bolometers for the on-chip detectors.

The beginning of this chapter motivates TES bolometers by juxtaposing them with competing technologies, specifically HEMTS and NTD bolometers, in order to highlight the deficiencies that TESs avoid. We discuss the principle of electrothermal feedback and derive stability criteria and sensitivity equations. Finally, we describe how the bolometers in this thesis were fabricated as well as the electronics used to read them. Throughout the chapter, we show data from dark measurements of our bolometers demonstrating acceptable transition temperatures, saturation powers, and time constants. We describe the cryogenic dewar used for these measurements in detail in Chapter 6.

3.2 Quantum Mechanics of Detection

The paper "Thermal Noise and correlations in photon detection" (*Zmuidzinas* [2003b]) provides a useful framework that motivates many of our own design decisions, including those in chapters 7 and 8. We refer the reader to this paper for a more detailed description and only summarize the relevant results here.

Detectors can be regarded as a circuit where photons incident on the input port $i = 1$ are created by operator $a_1^\dagger(\nu)$ and those at the output ports $j \neq 1$ (connected to bolometers) are created by operators $b_j^\dagger(\nu)$ given by:

$$b_j^\dagger(\nu) = S_{1j} a_1^\dagger(\nu) + c_j^\dagger \tag{3.1}$$

where $c_j^\dagger$ create noise photons at the bolometer j and S_{ij} is the scattering matrix discussed in Chapter 4. In the time domain, a bolometer in a pixel with low internal noise ($c_j^\dagger \approx 0$) receives power created by $b_i^\dagger(t) = \int_o^\infty d\nu \sqrt{h\nu} \exp(i2\pi\nu t) b_i^\dagger$. If the incident photons are thermal with distribution $\left\langle a_o^\dagger(\nu) a_o(\nu') \right\rangle = n_0(\nu)\delta(\nu - \nu')$ where $n_o(\nu)$ is a plank function, then over a time τ, the bolometers will receive energy

$$\begin{aligned} \langle d_i \rangle &= \tau \int_o^\infty \left\langle b_i^\dagger(t) b_i(t) \right\rangle \\ &= \tau \int d\nu h\nu \left| S_{i1}(\nu) \right|^2 n_o(\nu) \end{aligned} \tag{3.2}$$

with variance

$$\begin{aligned} \sigma_{ij}^2 &= \langle d_i d_j \rangle - \langle d_i \rangle \langle d_j \rangle \\ &= \tau \int d\nu (h\nu)^2 \left| S_{i1}(\nu) \right|^2 n_o(\nu) \delta_{ij} - \tau \int d\nu (h\nu)^2 \left| S_{i1}(\nu) \right|^2 \left| S_{j1}(\nu) \right|^2 n_o^2(\nu) \\ &= \tau \int d\nu (h\nu)^2 \left| S_{i1}(\nu) \right|^2 n_o(\nu) \left(\left| S_{i1}(\nu) \right|^2 n_o(\nu) + 1 \right) \end{aligned} \tag{3.3}$$

Equations 3.2 and 3.3 apply to direct detectors, including bolometers. Alternatively, a receiver can include a high frequency amplifier (like a High Electron Mobility Transistor, or

HEMT), but this contributes additional "quantum noise" through the operator $c_j^\dagger$. Quantum noise arises when the detector Nyquist samples incoming radiation, but suffers a noise penalty in power from the Uncertainty Principle while sampling on such a short time scale. These photons adds to the energy and covariance in Equations 3.2 and 3.3, the details of which are discussed in *Zmuidzinas* [2003b].

3.3 Competing Technologies to TES Bolometers

3.3.1 Coherent Receivers

The microwave background poses a unique decision tree to experimental cosmologists because it's statistical occupation number $n_{CMB} = (\exp(h\nu/kT) - 1)^{-1}$ is approximately unity for the frequencies of interest in most experiments. By contrast, optical astronomers typically observe radiation in the Wein Tail of a Plank distribution where $h\nu \gg kT$ and so $n \ll 1$. Meanwhile, radio astronomers often observe in the Rayleigh-Jean's limit where $h\nu \ll kT$, corresponding to a large occupation $n \gg 1$. While these limits motivate the researchers in each field to build very different styles of detectors, cosmologists observing the CMB work in the occupation number cross-over regime where both sets of detection techniques can be appropriate.

The Noise Equivalent Power (NEP) is the incident power required to achieve a signal-to-noise ratio of unity over 0.5s of integration. For a background-limited detector whose greatest source of noise is that present in the incoming radiation itself,

$$NEP^2 = 2(h\nu)^2 \Delta\nu \frac{n(\nu)(1 + \eta n(\nu))}{\eta} \tag{3.4}$$

where η is the efficiency of absorption and $\Delta\nu$ is the bandwidth (*Zmuidzinas* [2003b]). We can construct this equation from the ratio of Equations 3.2 and 3.3 evaluated in the special case of a two-port circuit with $|S_{12}(\nu)|^2 = |S_{21}(\nu)|^2 = \eta < 1$. If that same detector is preceded by HEMT, then all scattering matrix elements vanish except $|S_{21}(\nu)|^2 = G(\nu) \gg 1$,

representing a large gain. In this limit, the NEP (referenced to pre-amplified input power) reduces to

$$NEP^2 = 2(h\nu)^2 \Delta\nu \left(\frac{(1 + \eta n(\nu))}{\eta} \right)^2 \tag{3.5}$$

The noise for such a receiver includes not only the background noise, but also a residual quantum noise present even when the detector is kept dark with no incident radiation (*Zmuidzinas* [2003b]). The ratio of noise for direct (Equation 3.4) to coherent (Equation 3.5) detection is

$$\frac{NEP^2_{quantum}}{NEP^2_{direct}} = \frac{\eta n(\nu) + 1}{\eta n(\nu)}$$

If $n(\nu) \gg 1$, then the NEPs are equal and there is no penalty for coherent detection. However, for a background primarily of 2.7K CMB photons (in a spacecraft for example), this ratio exceeds two and the detector becomes quantum noise limited above 100GHz for most reasonable efficiencies.

Numerous researchers have justified using coherent systems by focusing on the Rayleigh Jeans portion of the spectrum or by using terrestrial telescopes whose loading is dominated by the atmosphere with an effective temperature $\sim 20K$ (e.g. TOCO, DASI, and QUIET). For temperature maps where the foregrounds could safely be ignored, this was a successful strategy. However, as mentioned in Section 2.10, the polarized foreground minimum is likely between 80 and 150 GHz, and experiments that control for scattering off dust will need to receive even higher frequencies. At these frequencies, quantum noise is unacceptably high for space or balloon borne experiments. Making matters even worse, HEMTs often operate with noise levels a factor of several higher than the quantum noise limit.

3.3.2 NTD-Ge Bolometers

All thermal radiation detectors used in direct detection schemes utilize an absorbing element with a heat capacity C. The absorber sits in weak thermal contact with a heat

bath through a conductive link with conductance $G \equiv \partial P/\partial T$. If the power deposited on the detector increases from P to P', then the absorber will approach a new temperature $T' = T + P'/G$ with a thermal time constant

$$\tau_o = \frac{C}{G} \tag{3.6}$$

We can determine the incident power P by measuring the detector temperature T'. Bolometers are a special class of thermal detector that use a thermistor to monitor this temperature (*Richards* [1994]).

One of the most successful bolometers used for millimeter and submillimeter detection is the NTD-Ge bolometer. These bolometers have a semiconducting Germanium thermistor whose band properties have been modified by Neutron Transmutation Doping (NTD). Experiments such as ACBAR, MAXIMA, and BOOMERanG, suspended these thermistors on released spiderweb-shaped absorbing structures in the back of horn antennas. The spiderwebs maintain the weak thermal link between the thermistor and heat-bath. They efficiently absorb the microwaves, but have a low cross section to cosmic rays.

The internal noise of most bolometers is dominated by phonon noise in the thermally conducting legs that connect the suspended absorber-thermistor structure to a surrounding heat bath:

$$NEP_G^2 = 4kT_{bolo}^2 G = \frac{4kT_{bolo}^2 P_{incident}}{T_{bath-T_{bolo}}}$$

This noise is minimized by operating the bolometer at roughly twice the bath temperature (*Richards* [1994]). For a focal-plane cooled with a ^{3}He sorption fridge, the bath temperature is roughly $T_{bath} \approx 250mK$, so most bolometers in systems like these are ideally operated at $T_{bolo} \approx 500mK$

The statistical noise associated with the incident photons' bose distribution is

$$NEP_\gamma^2 = 2\int P_{incident} h\nu d\nu + \int P_{incident}^2 d\nu$$

where the thermal blackbody distribution is

$$P_{incident} = \frac{2h\nu}{e^{h\nu/kT} - 1} \tag{3.7}$$

(*Pathria* [1996]) Typical optical loading on a terrestrial telescope from the CMB, atmosphere, and optics is between 5 and 20 pW, corresponding to a NEP_γ $10^{-16}W/\sqrt{(}Hz)$ (*Halverson* [2004]). By contrast, the typical thermal carrier noise in the legs is $NEP_G = 2\sqrt{(kT_{bath}P_{incident})} \sim 10^{-17}$. NTD Bolometers achieved background limited measurements in ground-based telescopes and were the state-of-the art detectors of the last decade.

Despite these successes, the NTD bolometers do have some short-comings. A telescope's mapping speed quantifies how long a unit area of the sky must be observed to achieve a desired signal to noise ratio. Once a telescope's detectors have been made background limited, the only way to increase the mapping speed is to increase the number of electromagnetic modes that the focal-plane recevies. Up to the throughput limit $A\Omega$ set by the focal-plane's area A and the telescope's field of view Ω, more modes can be received by increasing the number of detectors in the array. Numerous experiments that will map the CMB polarization over the next decade will have nearly 1000 detectors. However, NTD bolometers cannot be lithographed into monolithic arrays. Assembling kilopixel NTD arrays would be tedious, prone to poor yield, and require bulky mounting hardware that would inefficiently use the focal plane real estate compared to a monolithic array.

Additionally, if each detector in a kilopixel array were individually biased with separate lines, the wires would thermally load the 4K stage to an unacceptably high level. As a result, several research groups have started to use SQUID-based multiplexing (MUX) to read multiple detectors through one line. In these systems, some (or all) of the SQUIDs function as ammeters in series with voltage biased bolometers. However, the high impedance of NTD bolometers makes it impractical to operate in a voltage biased mode. Instead, researchers current bias the NTD bolometers and read the voltage with a JFET, but the bandwidth of most JFETs is too low for use in a MUX circuit (*Lanting* [2006]).

Finally, many proposed polarization experiments will rotate a half-wave plate at a few

hertz frequency in the optics between the secondary mirror and focal plane to control several systematic effects in the telescope. This scheme is only tenable if the detectors are robust against microphonic excitation. Mechanical vibrations can vary the distance between each of the bias wires or their distance to the ground plane, giving rise to capacitive fluctuations that act as a current source. The high impedance of NTD bolometers again creates a problem by converting this current into a very large voltage signal that contaminates the data time-stream. This effect proved to be a major challenge for the MAXIPOL project that continuously rotated a half-wave plate in front of an array of NTD bolometers (*Johnson et al.* [2003]).

3.4 TES Bolometers and Electrothermal Feedback

The Transition Edge Sensor (TES) bolometer is a new type of detector that addresses many of the above deficiencies (*Guildemeister* [2000]). Over the past five years, physicists have successfully deployed CMB-telescopes with TES-bolometers including APEX-SZ, ACT, and SPT and they will utilize TESs in several more instruments in the coming years including Polarbear, EBEX, BICEP-II, SPIDER, and the Keck Array.

A TES is a thin film of metal that is voltage biased into it's normal-superconducting transition (*Irwin and Hilton* [2005]). At these temperatures, the typical TES resistance is roughly 1Ω, making it robust against the vibrational pickup that plagues the NTD-Ge bolometers. Thanks to the low resistance, we can also use SQUID amplifiers to measure the current through the TES bolometers. The SQUIDs' high bandwidth naturally facilitates MUX readout schemes, alleviating thermal loading through the bias lines. Finally, we fabricate these detectors by lithographing and etching thin films of sputtered metals. As a result, we can build the densely populated monolithic arrays needed to scale up to kilopixel focal planes (*Chervenak et al.* [1999] and *Lanting et al.* [2005]).

Not only is the resistance of a TES low, but it changes rapidly with temperature in the transition. The dimensionless parameter

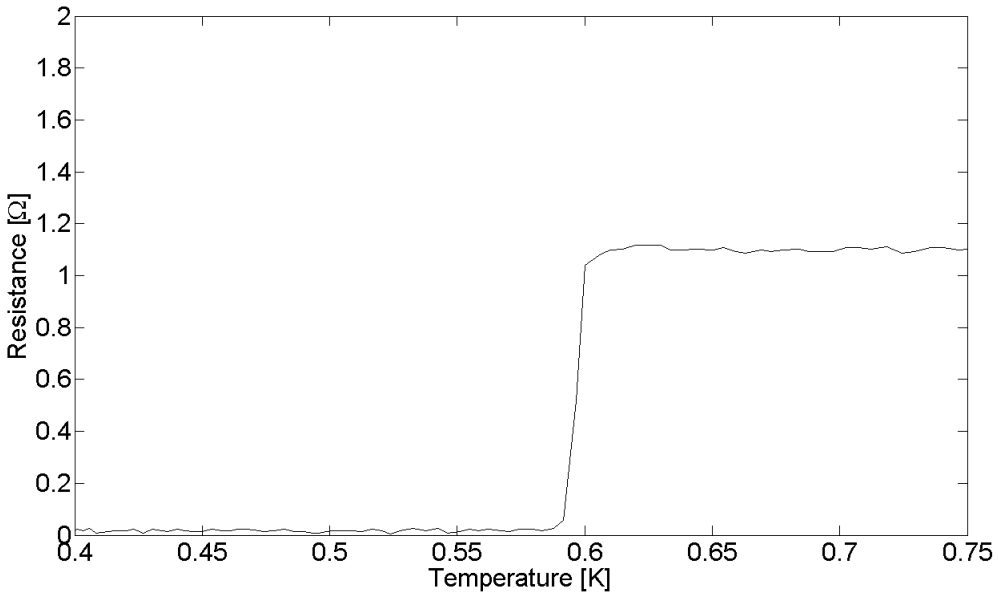

Figure 3.1. Resistance vs Temperature for a typical TES used in this thesis. This TES was unreleased, but was fabricated along-side fully functional bolometers. We monitored temperature with a Lakeshore GRT and measured the resistance with a four-point resistance bridge. For this film, $\alpha \approx 263$, $R_{normal} = 1.04\Omega$, and $T_c = 0.597K$

$$\alpha \equiv \frac{d(\log R)}{d(\log T)} = \frac{T}{R}\frac{dR}{dT}$$

characterizes the slope of this temperature dependence (*Richards* [1994]). While NTD-Ge bolometers have a negative α of order unity, TES bolometers have a positive α between 50 and 500.

Figure 3.1 shows the sharp change in resistance of a non-released TES vs temperature in the vicinity of the transition. In this measurement, we induced a gradual temperature drift in the entire mK-stage and monitored it with a Lakeshore Germanium Resistance Thermometer (GRT). We read both the GRT and TES resistances with a Bridge circuit to keep the power dissipated from the measurements far less than the power transmitted down the vespel legs of the mK-stage. Chapter 6 discusses the dewar design.

When biased into it's transition, small increases in optical loading P_{opt} induce small increases in the temperature of the TES. But thanks to the large positive α, these small

temperature changes create sizable increases in resistance. As a result, the joule heating from the bias circuit

$$P_{bias} = \frac{V^2}{R(T)}$$

drops. Conversely, decreases in the optical loading power induce increases in the joule heating power. This electrothermal feedback ensures a constant total loading power $P_{opt} + P_{bias}$ as the optical P_{opt} changes.

Energy conservation for thermal power flowing through the bolometer requires that

$$\begin{aligned} P_{opt} + P_{bias} - P_G &= \frac{dE}{dt} \\ P_{opt} + \frac{V^2}{R(T)} - GT &= \frac{dE}{dT}\frac{dT}{dt} \\ &= iC\omega T \end{aligned} \tag{3.8}$$

where the last line refers to a specific fourier mode of frequency ω. A change in P_{opt} will induce a change not only in the bolometer temperature T, but also the resistance R(T):

$$\begin{aligned} \frac{dT}{dP_{opt}} &= \left[i\omega C + \frac{V^2}{R^2}\frac{R}{T}\alpha + G \right]^{-1} \\ &= \frac{1}{G(1+\mathcal{L})(1+i\omega\tau)} \end{aligned}$$

where the definition of loop gain is analogous to that in electronic feedback systems:

$$\mathcal{L} \equiv -\frac{\partial P_{bias}}{\partial(P_{opt} + P_{bias})} = \frac{\alpha P_{bias}}{GT} \tag{3.9}$$

and the bolometer's time constant has decreased to

$$\tau = \frac{\tau_o}{\mathcal{L} + 1} \tag{3.10}$$

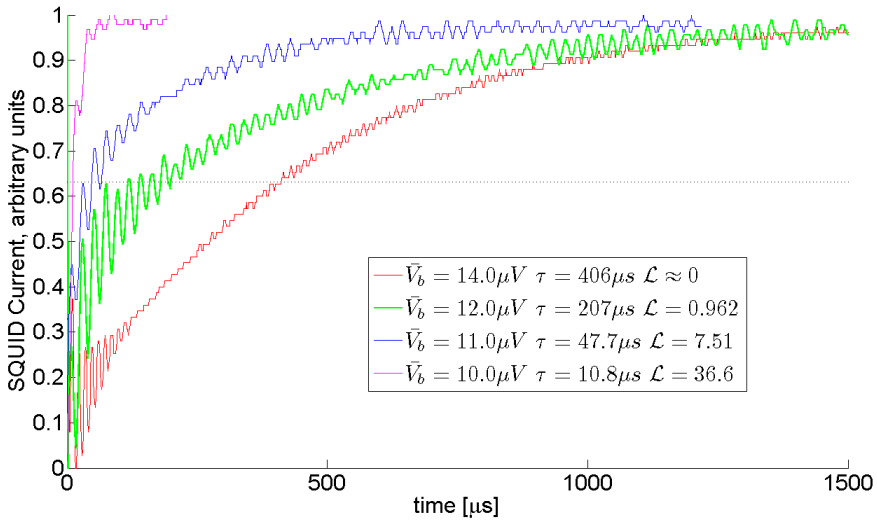

Figure 3.2. Arbitrarily normalized SQUID current vs time for a typical TES-bolometer. We biased the bolometers with the DC offset of an analog function generator carrying a small amplitude (2 μV) square-wave. As the bias passes through the transition point at 12 μV, the thermal time constant (Equation 3.10) drops dramatically. The red curve is well above the transition, the green is at the turn-around, and the purple is just above instability. The black dashed line guides the eye to the $1/e$ points.

Figure 3.2 shows measurements of the time constant at different bias voltages for a typical TES bolometer used in this thesis. When biased at it's IV-curve turn-around, the loop gain is 1 and the measured time constant is simply half of the thermal time constant given in Equation 3.6. These data suggest that the thermal time constant for our bolometers is $\tau_o \sim 400\mu s$, but that that deep in the transition we can speed it up with loop gains of $\mathcal{L} \sim 40$.

The SQUID reads the current through the voltage-biased TES, and the change in resistance alters this current:

$$\frac{\partial I}{\partial T} = \frac{\partial}{\partial T}\left(\frac{V}{R(T)}\right) = -\frac{\mathcal{L}G}{V}$$

So the sensitivity for the detector is

$$s \equiv \frac{dI}{dP_{opt}}$$
$$= \frac{\partial I}{\partial T}\frac{\partial T}{\partial P_{opt}} = -\frac{1}{V}\frac{\mathcal{L}}{\mathcal{L}+1}\frac{1}{1+i\omega\tau}$$

If we observe optical signals changing slowly ($\omega \ll 1/\tau$) with a detector operating deep in its transition ($\mathcal{L} \gg 1$), the changes in P_{bias} will exactly compensate the changes in P_{opt}. In this strong-electrothermal feedback limit, the sensitivity is simply

$$s \simeq -\frac{1}{V} \tag{3.11}$$

and the detector response is linear over a wide range of optical loading, independent of the bolometer's physical properties (*Guildemeister* [2000]).

TES-bolometers have a distinctive IV-curve that is linear in it's resistive regime, but "turns around" when the voltage bias is sufficiently low that the bolometer enters it's transition (See figure 3.3). In the transition, the resistance drops rapidly enough that further decreases in bias voltage actually cause increases in current. Deep in the transition, this power is held constant, resulting in a PV-curve that is flat in the transition (See figure 3.4). For a dark measurement such as that in Figure, $P_{opt} = 0$ and the power dissipated in the transition must equal P_G carried away through the legs. P_G is often called the saturation power P_{sat} because if the total power dissipated in an optically active bolometer exceeds P_{sat}, it will climb out of it's transition and be driven normal. The range of linearity of a TES is thus limited to $P_{tot} = P_{bias} + P_{opt} < P_{sat}$.

3.5 Fabrication

We fabricate our bolometers on 10-cm diameter 0.5mm thick silicon wafers and a picture of one is shown in Figure 3.5. The suspended TES sits on a 10000Å thick film of Low Stress silicon Nitride (LSN). While a 1 μm film of stoichiometric Silicon Nitride (Si_3N_4) can have an internal stress of a few GPa, the silicon rich LSN typically has an internal stress of only

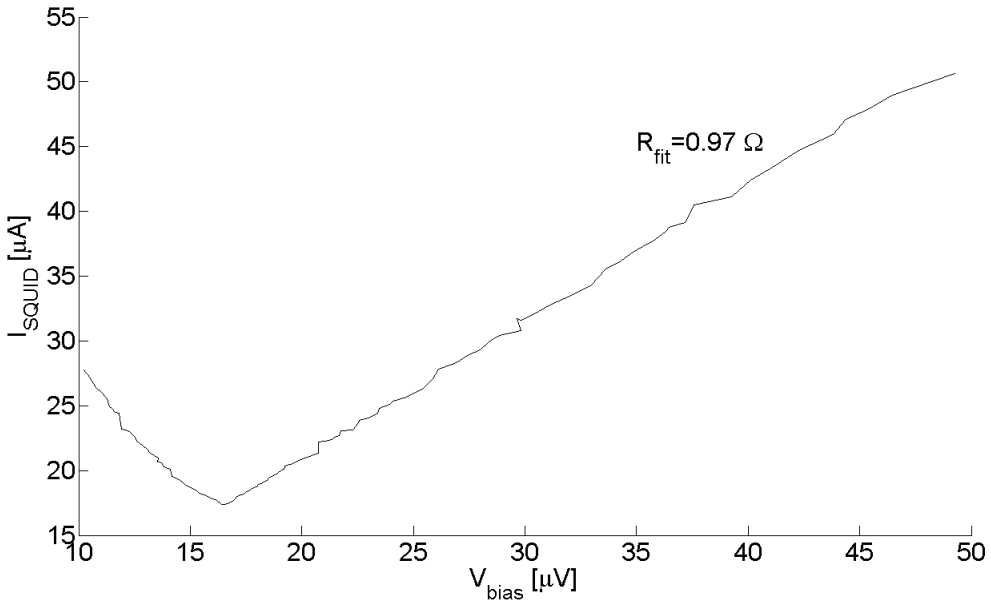

Figure 3.3. Plot of SQUID current vs bias Voltage for a 220GHz Dark Bolometer. The resistive portion of the curve is 0.97 Ω. This Bolometer was designed to receive 30% bandwidth at 220GHz.

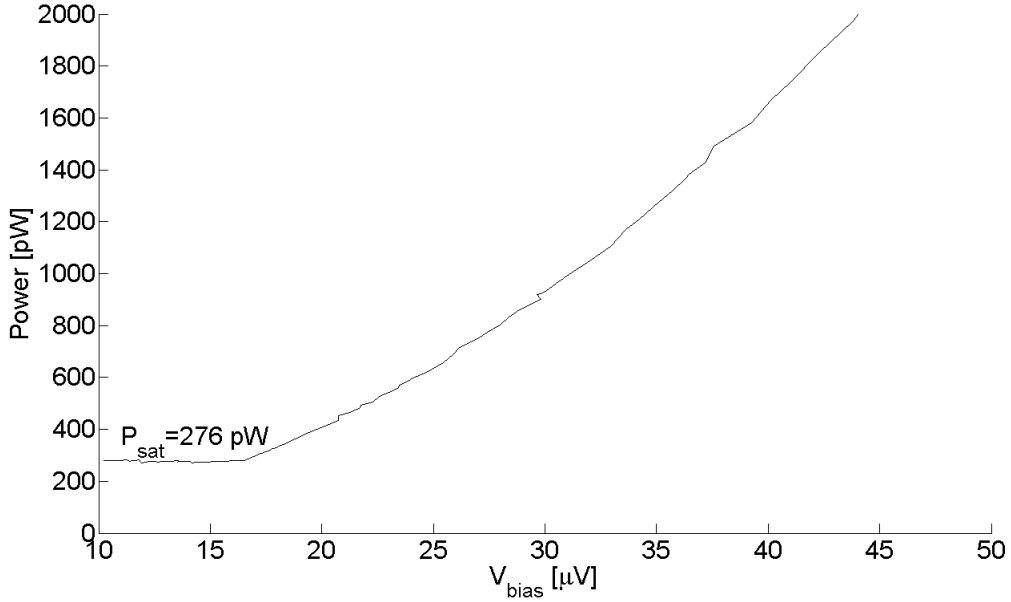

Figure 3.4. Plot of Power dissipated in the bolometer from Figure 3.3 vs bias Voltage for a 220GHz Dark Bolometer. The saturation power in the strong electrothermal feedback regime is 276pW for this bolometer, so we had to use an optical attenuator to avoid saturation when looking at room-temperature.

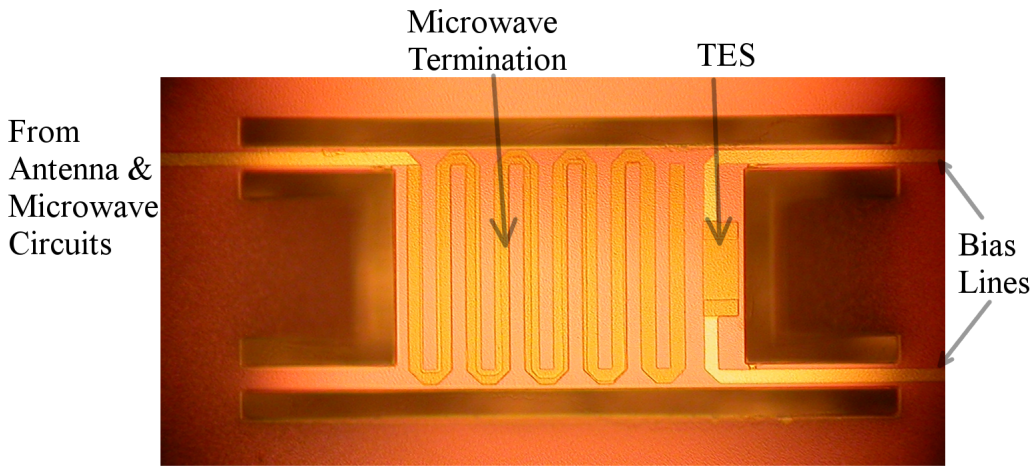

Figure 3.5. Released TES bolometer. The out-of-focus regions are silicon several microns below the released bolometer.

100 MPa (*Chang* [2010c]). A bolometer with higher stress would not survive the release procedure described below.

The TES is comprised of an aluminum-titanium bilayer with sputtered 400 Å Aluminum (Al) covering 800 Å Titanium (Ti) (*Chang* [2010a]). Aluminum's superconducting transition temperature of $T_c = 1.2K$ is too high to minimize phonon noise to a 250 mK heat bath. The titanium, whose $T_c = 0.39K$ decreases the bilayer's effective transition temperature to $\approx 500mK$ by the proximity effect. Cooper pairs from the Al leak into the otherwise normal Ti and quasiparticles from the Ti leak into the aluminum, resulting in a lower transition temperature. The proximity effect is strongest when the bilayer thickness matches the cooper pair coherence length (*Werthamer* [1963]). We chose the total film thickness of 1200 Å to ensure efficiently proximitizing and chose the Ti:Al thickness ratio of 2:1 to give the desired $T_c \approx 500mK$. Measurements suggest this was a little higher, closer to $T_c \sim 600mK$ (see Figure 3.1).

We fabricated both the microstrip circuits that couple optical power to the bolometer and the bolometer bias lines from the same 6000 Å thick film of Niobium (Nb), whose transition temperature is nominally $T_c = 8.2K$ (*Van Duzer* [1998]). The power in the

microstrip circuits terminates on resistive loads and lossy transmission lines that are in tight thermal contact with the TES and were etched from the same Al-Ti bilayer as the TES. We defer the discussion of the microwave designs on sky-side of the resistive until later chapters.

We etched holes through the LSN around the bolometers with an SF_6 plasma and used a Xenon-diflouride (XeF_2) gas to attack and remove the Silicon from under the bolometer, leaving a suspended structure (*Chang* [1998]). Our goal was to realize the suspension legs that carry a sufficiently high power to prevent the detectors from saturating when the cryostat looked at a 300K thermal load. The power flowing through each leg is

$$P(x) = Ak(T)\frac{dT}{dx}$$

In addition to the LSN, the legs have films of 3000Å Nb, 5000Å SiO_2, and 6000Å Nb. Since the Nb is superconducting, the only conduction should be through phonons whose heat conductivity $k(T) = k_o T^3$ ((*Van Duzer* [1998])), so the power flowing down N legs of length L and cross sectional area A integrates to:

$$P_G = N\frac{Ak_o}{4L}(T_{TES}^4 - T_{bath}^4) \tag{3.12}$$

We attempted to use Equation 3.12 to tailor our bolometer legs from previously measured saturation powers of Polarbear detectors. Ideally, we would have built our bolometers to have $P_G = P_{tot} > 2P_{opt,max}$ for the maximum possible loading to ensure they would not saturate. In the Rayleigh-Jean's limit, a single polarization of incident Power in Equation 3.7 is summed across a square band of width $\Delta\nu$ provides a loading

$$P_{opt} = \eta k T \Delta\nu \tag{3.13}$$

where η is the total receiver's efficiency. With 30% fractional bandwidths and *perfect efficiency*, the optical loading powers from a 300K source range from 111pW to 277pW for our detectors.

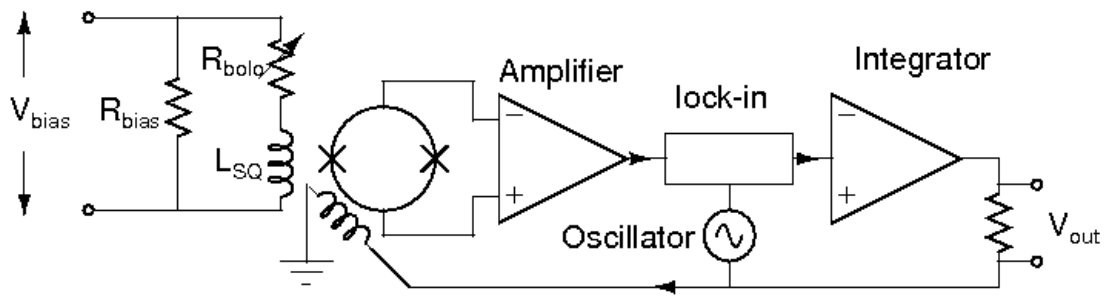

Figure 3.6. SQUID readout electronics. The electronic to the left of the SQUID were made in Berkeley for our test-system. The warm electronics to the right of the SQUID use a lock-in amplifier and a feed-back loop to reduce noise and linearize the SQUID. The details of the warm circuitry are not shared by the manufacturer, Quantum Design Corp.

Unfortunately, many of our detectors' measured saturation powers were less than twice this maximum loading. Table 3.1 summarizes the Chapter 8 bolometers' thermal properties. For reference, the right column is twice the maximum anticipated optical loading without any attenuation. To remedy this problem, we had to use an optical attenuator to shade our detectors for those measurements. Our Bolometers are significantly larger than the Polarbear bolometers, so we suspect that we experienced low saturation power because to achieve full release , we etched our devices with XeF_2 100-150% longer. This longer etching likely thinned the legs and depressed the saturation powers. The bolometers in chapter 6 were of comparable size to the Polarbear detectors and did not saturate; their saturtion powers all exceeded twice their maximum loading.

Table 3.1. Measured Thermal Characteristics of Ch 8 Bolometers

f_o [GHz]	τ_o [μs]	P_{sat} [pW]	$2P_{opt,max}$ [pW]
86	406	155	224
104	336	190	258
126	296	208	312
151	256	231	376
183	246	253	454
222	222	277	550

3.6 Bolometer stability and readout electronics

The bolometers in this thesis are in series with an input coil with inductance L that magnetically couples to Superconducting QUantum Interference Devices (SQUIDs). Our DC-SQUDIS were purchased from the Quantum Design Corporation, which operate in an AC flux-locked-loop mode (see Figure 3.6)

We biased the bolometers with a 6V battery box and varied the applied voltage with potentiometers. That voltage was further divided between a warm $2k\Omega$ reference resistor and a 4K bias resistor R_{bias} in parallel with both the bolometer (R_{bolo}) and the SQUID input coil (see Figure 3.6 for the 4K portion of this electronics). We chose the value of $R_{bias} = 0.02\Omega$ to ensure that the bias circuit applies $V_{bias} = 1 - 60\mu V$ across the bolometer for 0.1-6V voltage drops measured across the warm $2k\Omega$ resistor. This applied bias voltage

$$V_{bias} = L\frac{dI}{dT} + IR(T)$$

is coupled to the thermal equations 3.8 through the temperature dependence in the resistance (*Irwin and Hilton* [2005]). Expanding the variables I, P, V, and T to first order about their DC values, the resistance is:

$$R = R_o(1 + \alpha\frac{\partial T}{To})$$

and the thermal equations become:

$$\begin{aligned} P_G &= P_{Go} + G\partial T \\ P_{bias} &= P_{Jo} + 2I_oR_o\partial I + \frac{1-\mathcal{L}}{\tau_o}\partial T \end{aligned} \tag{3.14}$$

Without the DC therms, Equations 3.14 are:

$$\frac{d}{dt}\begin{pmatrix} \partial I \\ \partial T \end{pmatrix} = \begin{pmatrix} \frac{1}{\tau_{el}} & \frac{\mathcal{L}G}{I_oL} \\ -\frac{2I_oR_o}{C} & \frac{1}{\tau'} \end{pmatrix} \begin{pmatrix} \partial I \\ \partial T \end{pmatrix} + \begin{pmatrix} \frac{\partial V}{L} \\ \frac{\partial P}{C} \end{pmatrix} \tag{3.15}$$

where $\tau_{el} = L/R$ is the electrical circuit's time constant and $\tau' = \tau_o/(\mathcal{L}-1)$. The homogeneous solutions of Equation 3.15 have the form $\partial T_{hom} \propto A_+ V_+ e^{-t/\tau_+} + A_- V_- e^{-t/\tau_-}$, where the eigenvalues are

$$\frac{1}{\tau_\pm} = \frac{1}{2}\left[\frac{1}{\tau_{el}} + \frac{1}{\tau'} \pm \sqrt{\frac{1}{\tau_{el}} - \frac{1}{\tau'} - 8\frac{R_o\mathcal{L}}{L\tau_o}}\right]$$

The solutions are stable and will relax back to the DC values provided that the real part of the eigenvalues are positive. If it is critically damped ($\tau_+ = \tau_-$), then the solutions will still be stable provided that the circuit inductance L is between the critical values:

$$L_\pm = \left(1 + 3\mathcal{L} \pm \sqrt{2\mathcal{L}(1+\mathcal{L})}\right)\frac{R_o\tau}{(\mathcal{L}-1)^2}$$

In the strong electro-thermal feedback limit, $\mathcal{L} \gg 1$ and this reduces to the condition that the inductance L must be between

$$L_\pm/R_o = \left(3 \pm 2\sqrt{2}\right)\frac{\tau}{\mathcal{L}}$$

which is the well known condition that the electrical time constant must exceed the thermal one (sped by feedback) by at least 5.8 to ensure stability (*Irwin and Hilton* [2005]). Our Quantum Design SQUIDS have an input inductance of $2\mu H$, which means the electrical time constant with a 0.02Ω resistance is $100\mu s$. While this is indeed less than the bolometer's typical thermal time constant of $\sim 400\mu s$ (no feedback), it is insufficient in the transition where we have achieved loop gains of nearly 40, and hence thermal time constants drop to $\sim 10\mu s$.

For multiplexed arrays, our group combats a similar stability problem by adding 1-2 μm thick films of gold onto the bolometer islands to add heat capacity and drastically increase the thermal time constants (*Mehl et al.* [2008]). However, the devices in this thesis are only prototype devices read with non-multiplexed DC SQUIDS and stimulated with very 100K bright signals. Since the gold-deposition complicates the fabrication process,

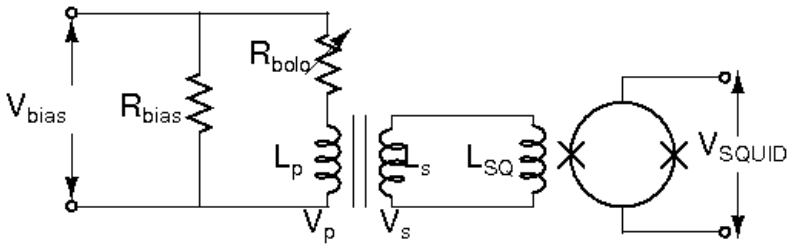

Figure 3.7. Circuit diagram the cold section of our electronics. The output V_{SQUID} is processed further by the electronics in the warm control circuit shown in Figure 3.6. We have inserted a hand-wound transformer, where the coil in DC contact with the bolometer has inductance L_P and the coil in DC contact with the SQUID pickup inductor has inductance L_S.

we alternatively modified the bias circuit to decrease τ_{el} by installing a superconducting transformer (see Figure 3.7) between the bolometer and the SQUID input coil (L_{SQ}).

If the primary and secondary coils have N_p and N_s windings, with corresponding self-inductances L_p and L_s, then the voltage on the secondary is

$$V_s = \frac{N_s}{N_p} V_p = \sqrt{\frac{L_s}{L_p}} V_p.$$

The current fed through the SQUID input coil is

$$\begin{aligned} I_{SQ} &= \frac{V_s}{i\omega(L_s + L_{SQ})} \\ &= \frac{\sqrt{L_s/L_p}}{i\omega(L_s + L_{SQ})} V_p \\ &= \frac{\sqrt{L_s/L_p}}{i\omega(L_s + L_{SQ})} (i\omega L_p I_{bolo}) \end{aligned}$$

So

$$\frac{I_{SQ}}{I_{bolo}} = \frac{\sqrt{L_p L_s}}{L_s + L_{SQ}} \tag{3.16}$$

(*Guildemeister* [2000]).

We hand-wound transformers with Nb wire around a 1.5mm diameter teflon tube with

a N_p : N_s=15:10 ratio of windings, resulting in a drop in current of 1/4 (in Equation 3.16) from the bolometers to SQUIDs, and a corresponding jump of 4 in voltage. As a result, the bolometers see an impedance and hence inductance that was 16 times lower than it would with just the bare SQUID, providing an electrical time constant that was much less than the thermal one. Operated with these transformers, the bolometers were stable. We determined the coupling efficiency of our transformer-coupled SQUIDs by measuring the IV curves' slopes for metal-mesh resistors in lieu of bolometers. These resistors had a previously measured 4K resistance of $R \sim 0.5\Omega$, so the efficiency is simply the ratio of the IV curve slope to the expected $2\mho$ that would have arisen if $I_{SQ} = I_{bolo}$.

The factor of 4 penalty in signal means that this solution is only acceptable for prototype devices that will never be used in the field where high sensitivity is required. However, for the prototyping described in this thesis where the detectors were stimulated with bright sources (100K), this loss is acceptable provided that it is understood.

3.7 Conclusions

This chapter discussed the theory of TES bolometers and explained the advantages they offer over competing technology. We described the fabrication, readout electronics, and dark tests of bolometers. These bolometers were integrated into the microwave circuits as high-sensitivity power meters described in later chapters.

Since this thesis seeks to explore broadband optical coupling schemes, TES bolometers are not a unique choice for this prototyping work. In principle, the microwave electronics described in later chapters could be coupled to a wide range of detectors including MKIDS, SIS-junctions, or even old fashioned NTG-bolometers. Some of the prototyping described in chapter 5 was even done warm at 1-10GHz with diodes and network analyzers. Additionally, the multichroic pixels will demand readout capable of supporting 3-10 times more channels per pixel that existing focal planes use, which makes MKIDS a compelling detector option in the future.

However, the microwave structures have been designed with CMB-polarimetry in mind

and TES-bolometers are currently the technology of choice in these measurements for the reasons outline above. As a result, it is necessary to integrate our antennas and filter networks with TES-bolometers in order to prove their viability to the other researchers in the field. This is demonstrated in chapters 6,7 and 8.